(Received 7 January 2024, Accepted 28 February 2024, Scheduled 8 March 2024)

A Compact Loop-Shaped Dual-Band Omnidirectional Rectenna for RF Energy Harvesting

Lei Li*, Ruifeng Xu, Jingxu Cao, Xue Li, and Jingchang Nan

School of Electronics and Information Engineering, Liaoning Technical University, Huludao 125105, China

ABSTRACT: This paper presents a compact loop-shaped omnidirectional rectenna for RF energy harvesting at 2.45 GHz and 5.8 GHz. Firstly, a loop-shaped antenna with iterated circular concave and convex structures is proposed to operate at both frequencies. Then, a rectifier circuit uses a complex impedance correlation matching technique to achieve high conversion efficiency. By connecting a piece of microstrip, two uncorrelated input impedances are transformed into a pair of conjugate impedances. In addition, by using a Π-shaped structure with the same equivalent characteristic impedance and complementary equivalent electrical lengths at both frequencies, the pair of conjugate impedances are simultaneously matched to 50 Ω. The rectifier circuit is integrated in the loop-shaped antenna to form a compact dual-band rectenna. The overall size of the rectenna is 67.5 mm × 71.5 mm × 1.016 mm. The test results show that the S_{11} of the antenna is −13.5 dB and −18.7 dB, and the peak conversion efficiencies of the rectenna are 65.1% and 38.4% at 2.45 GHz and 5.8 GHz, respectively. The simulated and tested results are quite similar.

1. INTRODUCTION

As the Internet of Things and communications technology are developed, compact low-power devices such as wireless sensors have been widely used in various aspects [1]. Because batteries powering low-power devices are lifetime-limited and challenging to replace, a wireless method is required to power wireless sensors and other devices. Conventional wireless energy, including wind, solar, and mechanical energy, is significantly impacted by environmental factors. Hence, it is unsuitable for providing consistent power to distributed sensors [2]. Wireless Power Harvesting (WPH) technology can solve the problem, which harvests low-density electromagnetic energy from free space and converts it into DC power [3]. At the same time, with the proliferation of communications base stations, WLAN and electronic transceivers, a great deal of electromagnetic energy is filled in the environment. WPH is therefore a viable solution for providing power to devices with low power consumption.

Rectenna is the primary component of WPH system, which consists of an antenna and a rectifier circuit. The antenna captures RF energy, while the rectifier circuit converts the RF energy into DC energy. In recent years, many results have been proposed for rectennas operating in different frequency bands, such as single-frequency, multi-frequency [4, 5], and wideband. A harmonic suppression rectenna operating at 2.45 GHz is described in [6]. Harmonic suppression is achieved by adding two microstrip stubs to the antenna feed line. When the input power is 18 dBm, the peak conversion efficiency of the rectenna is 65%. In [7], a compact rectenna operating at 2.45 GHz is proposed, consisting of a patch antenna, a diode, and a section of shortend microstrip line connected in series. ing at 2.45 GHz is presented in [8]. The differential fed microstrip antenna is connected directly to the rectifier circuit, eliminating a matching network. The rectenna achieves a peak conversion efficiency of 73.9% at a power density of 207 μ/cm^2. Even though the single-frequency rectenna can increase the conversion efficiency by using differential feed, harmonic suppression and other methods, higher input power is required. In contrast, RF power density is extremely low in the physical environment. Therefore, some researches have employed broadband and multi-frequency rectenna to harvest more energy. A four-band flexible rectenna operating at 900 MHz, 1800 MHz, 2.45 GHz, and 5.8 GHz is proposed in [9]. The receiving antenna adopts a novel feeding structure composed of coplanar waveguide and transition section, and the rectifier circuit adopts a matching network based on a cross-shaped bending short line to realize broadband. The size of the rectenna is 105 mm × 82 mm × 0.125 mm, and the conversion efficiencies at four frequencies are 48%, 50%, 42%, and 34%, respectively. A seven-band omnidirectional rectenna operating in GSM1800, LTE, WLAN, and 5G bands is proposed in [10]. The seven-band rectifier circuit consists of three optimized single shunt diode rectifiers circuits in parallel, and each sub-rectifier circuit operates in two or three frequency bands. In addition, an omnidirectional monopole antenna is designed to match the circuit. The size of the rectenna is 92 mm × 54 mm × 0.787 mm, and the conversion efficiency of the rectenna is 28.3%–45.4% under seven operating frequency bands. An ultra-wideband (UWB) rectenna operating at 0.9–3 GHz using a broadband complementary matching stub is presented in [11]. The rectenna size is 60 mm × 200 mm × 0.787 mm, and conversion efficiency is 50% over the entire frequency band. Although the above rectenna can cover many frequency bands, the rectifier circuit has lower conversion efficiency, complex structure, and large size. However, the dual-band rectenna combines the benefits

* Corresponding author: Lei Li (lilei_dx@lntu.edu.cn).

TABLE 1. Parameters of dual-band loop-shaped antenna.

Parameters	Value/mm	Parameters	Value/mm	Parameters	Value/mm
b	28.6	e	9.8	a_1	19.2
L	71.5	f	1.6	s	16.7
k	4.75	c_1	5.8	c_2	4.7
W	67	d_1	2.5	d_2	2.3

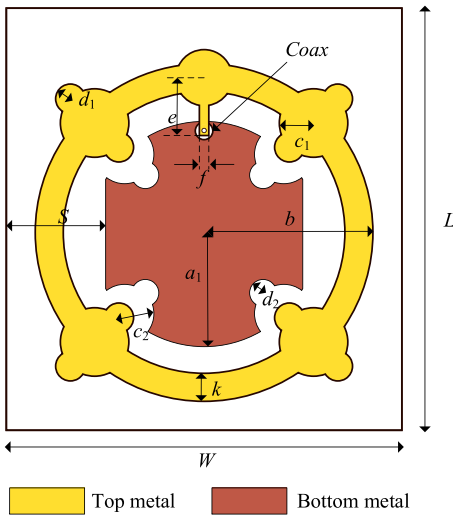

FIGURE 1. Layout of dual-band loop-shaped antenna.

of both with smaller size, wider frequency band, and higher conversion efficiency. In [12], a differential rectenna operating at 2.4 GHz and 5.5 GHz is described. The antenna consists of two concentric square patches, and the rectifier circuit is connected to the antenna radiation patch via a probe. The dimension of rectenna is 75 mm × 75 mm × 0.8 mm, and the conversion efficiencies are 36% and 8%, respectively. In [13], a rectenna operating at 2.45 GHz and 5.48 GHz is proposed. The antenna consists of a dual-layer substrate, fed by coax and connected to the rectifier circuit on the back of the bottom substrate via a probe. The rectenna dimension is 85.6 mm × 64 mm × 9.2 mm, and the conversion efficiencies at the two frequencies are 56.3% and 37.8%, respectively. A high gain rectenna operating at 3.5 GHz and 5.8 GHz is described in [14]. Utilizing an aperture-coupling feed, the antenna is constructed upon a multilayer substrate. The rectifier circuit is connected to the antenna via an SMA connector. The dimension of the rectenna is 95 mm × 65 mm × 5 mm, and the conversion efficiencies at the two frequencies are 44% and 29%, respectively. The rectennas mentioned above have high conversion efficiencies, but the rectifier circuits and antennas are discrete or multilayered, resulting in an enormous dimension and a high profile.

To solve the above problems, a compact dual-band omnidirectional rectenna operating at 2.45 GHz and 5.8 GHz with a rectifier circuit integrated in the loop-shaped antenna is proposed in this paper. The antenna realizes the dual-band omnidirectional radiation characteristics by adding iterated circular convex structures on the radiation patch and etching iterated circular concave structures on the ground plane. The rectifier circuit employs a Π-shaped network in series with a microstrip line for matching and a dual-radial stub DC pass filter for suppressing the fundamental frequency. To make the overall layout of the rectenna compact and small in size, the designed rectifier circuit is printed in the center blank area of the loop-shaped antenna. The size of rectenna is 67 mm × 71.5 mm × 1.016 mm. The tested impedance bandwidths of the proposed antenna are 2 ∼ 2.56 GHz, 3.75 ∼ 4 GHz, and 5.15 ∼ 6.28 GHz. The tested peak conversion efficiencies of the rectenna are 65.1% and 38.4% at 2.45 GHz and 5.8 GHz, respectively. The tested results show that the proposed idea can effectively reduce the overall size without affecting the performance of the rectenna.

2. DESIGN OF DUAL-BAND ANTENNA

2.1. Antenna Model

The layout of a dual-band loop-shaped antenna is depicted in Fig. 1, which consists of a loop-shaped radiation patch and a defective ground plane. Radiation patch and defective ground plane are printed on an F4B substrate ($\varepsilon_r = 4.4$ and $\tan\delta = 0.0033$) with dimension of 67.5 mm × 71.5 mm × 1.016 mm. The optimized parameters are depicted in Table 1.

2.2. Antenna Design

The rectenna employs an omnidirectional antenna to capture more RF energy, as RF energy in the natural environment radiates in all directions. The design procedure of the dual-band omnidirectional antenna is shown in Fig. 2. Antenna 1 is formed of a loop-shaped radiation patch and a circular ground plane, which is fed through a coaxial probe, as indicated in Fig. 2(a). The loop-shaped radiation patch is connected to the microstrip line through a circular structure to reduce the return loss caused by abrupt shape changes. Fig. 3 shows the impedance bandwidth of the antenna, and it can be seen that antenna 1 only resonates at 2.45 GHz. Fig. 4 demonstrates the current distribution of the antenna, with antenna 1 having stronger currents on the loop-shaped patch at 2.45 GHz. Fig. 4(b) presents that when antenna 1 is at 5.8 GHz, the current is stronger at ±45° and its diagonal positions, while it is weaker at other positions. Therefore, to excite resonance at 5.8 GHz, iterated circular convex structures are added at ±45° and their diagonal position on the loop-shaped patch of antenna 1 to alter the current path. At the same time, because the defect ground can enhance matching, iterated circular concave structures are into the circular ground plane, as shown in Fig. 2(b). Antenna 2 produces two desired resonance frequencies at 2.4 GHz and 5.8 GHz and an undesired resonance frequency at 4 GHz. Fig. 4(e) shows that the current of antenna 2

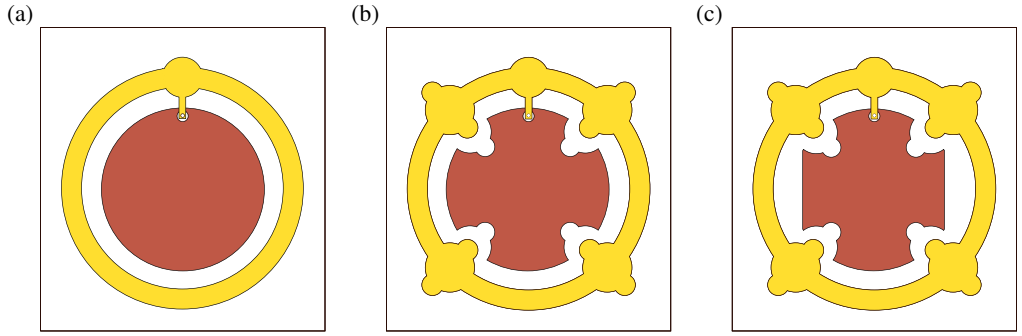

FIGURE 2. Three different structures of the proposed antenna, (a) antenna 1, (b) antenna 2, (c) antenna 3.

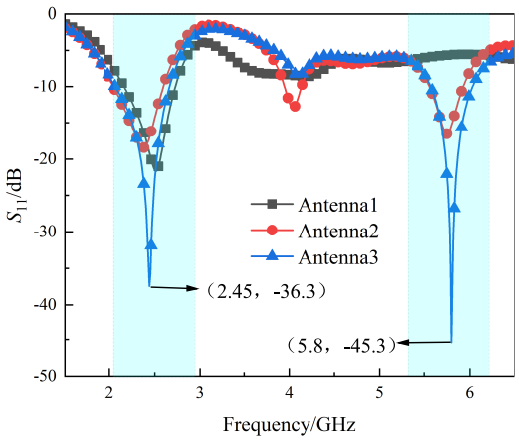

FIGURE 3. S_{11} of three different antennas.

is mainly distributed on the inner side of the loop-shaped patch between the two convex structures at 4 GHz. Then, to suppress the undesired resonance frequency, the right and left circular edges of the ground plane are truncated to rectangular edges to reduce the matching performance of antenna 2 near 4 GHz, as depicted in Fig. 2(c). As can be seen in Fig. 4(h), the current between the two concave structures on one side of antenna 3 is obviously reduced, and the matching performance around 4 GHz is weakened. S_{11} of the three different antennas of Fig. 2 are illustrated in Fig. 3. The S_{11} of antennas gradually decreases at 2.45 GHz and 5.8 GHz, and increases at 4 GHz with the evolution of the antenna. Antenna 3 resonates at 2.45 GHz and 5.8 GHz with S_{11} of -36.3 dB and -45.3 dB, respectively, while S_{11} is larger than -10 dB at 4 GHz.

Since the radii c_1 of the convex structures on the loop-shaped patch and c_2 of the concave structures on the defective ground significantly affect the resonance of the antenna 3, the values of c_1 and c_2 are optimized. Fig. 5 shows the S_{11} of antenna 3 for different radii c_1 and c_2, respectively. As c_1 increases, the two resonance frequencies of antenna 3 move towards lower frequencies. When $c_1 = 5.8$ mm, the resonance frequencies of antenna 3 are located at 2.45 GHz and 5.8 GHz, as shown in Fig. 5(a). As c_2 increases, the S_{11} of the antenna 3 decreases and then increases, and S_{11} is minimized when $c_2 = 4.7$ mm, as indicated in Fig. 5(b). The optimized values for antenna 3 are $c_1 = 5.8$ mm and $c_2 = 4.7$ mm. Fig. 6 depicts the radiation pattern of antenna 3, which is omnidirectional at 2.45 GHz and quasiomnidirectional at 5.8 GHz. The radiation pattern indicates that the design can receive RF energy from all directions.

3. RECTIFIER CIRCUIT ANALYSIS AND DESIGN

3.1. Rectifier Circuit Design

In this paper, a dual-band rectifier circuit working at 2.45 GHz and 5.8 GHz is designed to integrate in the loop-shaped antenna. The substrate of the rectifier circuit is identical to the antenna. Fig. 7(a) depicts the schematic diagram of the rectifier circuit, which is composed of four components: rectifier network, DC pass filter, matching network, and a load.

The rectifier network utilizes a doubled-voltage rectifier network with HSMS 2852 diodes D_1 and D_2 for high DC voltages. In order to obtain pure DC power, a dual-band DC pass filter is placed at the output terminal of the rectifier network. The DC pass filter utilizes three microstrip transmission lines and two radial stubs. By changing the dimension of the microstrip transmission lines and radial stubs, the input impedance can be adjusted to prevent the fundamental frequency energy from passing through the load. Because the input impedances of the rectifier circuit are different at the two frequencies represented with f_1 and f_2, the input impedances can be denoted as $R_1 + jX_1$ at f_1 and $R_2 + jX_2$ at f_2. The matching network is needed to match the two different input impedances to 50 Ω at the same time. Firstly, a section of microstrip line TL_4 is inserted in front of the rectifier network to generated two conjugated impedances at f_1 and f_2, shown as Fig. 7(a). The input impedance $Z_{in1}(f_1)$ and $Z_{in1}(f_2)$ of the rectifier network in series with TL_4 at two frequencies can be calculated using Equations (1) and (2).

$$Z_{\text{in1}}(f_1) = Z_1 \times \frac{(R_1 + jX_1) + jZ_1 \tan\theta_1}{Z_1 + j(R_1 + jX_1)\tan\theta_2} \quad (1)$$

$$Z_{\text{in1}}(f_2) = Z_1 \times \frac{(R_2 + jX_2) + jZ_1 \tan\theta_2}{Z_1 + j(R_2 + jX_2)\tan\theta_2} \quad (2)$$

where Z_1 is the characteristic impedance of TL_4, and θ_1 and θ_2 are the electrical lengths of TL_4 at f_1 and f_2, respectively.

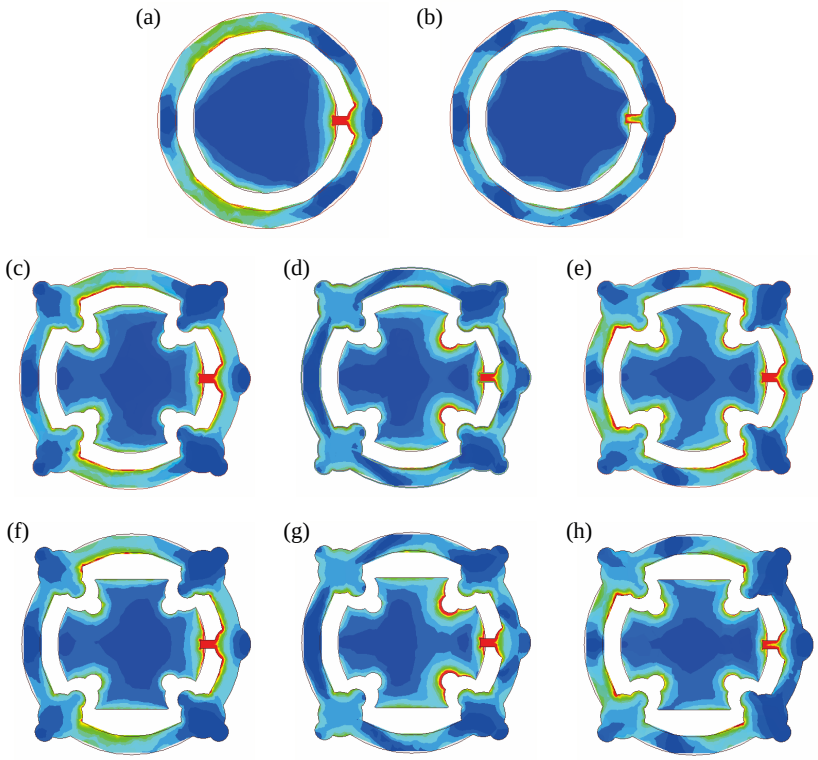

FIGURE 4. Current diagram of the (I) Antenna 1 (a) 2.45 GHz, (b) 5.8 GHz; (II) Antenna 2 (c) 2.45 GHz, (d) 5.8 GHz, (e) 4 GHz; (III) Antenna 3 (f) 2.45 GHz, (g) 5.8 GHz, (h) 4 GHz.

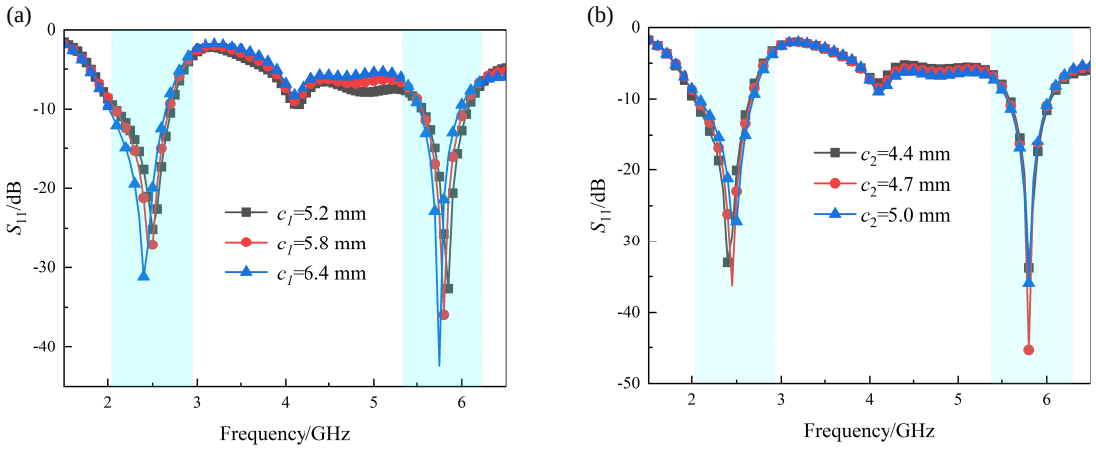

FIGURE 5. Simulated S_{11} for different (a) c_1 and (b) c_2.

Because $Z_{\text{in1}}(f_1)$ and $Z_{\text{in2}}(f_2)$ are conjugate, and there is proportional relation between θ_1 and θ_2, the Z_1 and θ_1 of TL_4 can be calculated from Equations (3) and (4).

$$Z_1 = \sqrt{R_1R_2 + X_1X_2 + \frac{X_1 + X_2}{R_2 - R_1}(R_1X_2 - R_2X_1)} \quad (3)$$

$$\theta_1 = \frac{f_1}{f_1 + f_2}\left\{\arctan\left[\frac{Z_1(R_1 - R_2)}{R_1X_2 - R_2X_1}\right] + n\pi\right\}, \quad n = 0, 1, 2, \ldots \quad (4)$$

In general, n can be arbitrary integers. However, when we choose the value of n, we should make TL_4 easy to be fabricated. Then, to match two mutually conjugated impedances to 50 Ω, a Π-shaped matching network is designed, which can be equivalent to two section microstrip lines with the same characteristic impedance and complementary electrical lengths at f_1 and f_2, shown in Fig. 7(b). The parameters of the Π-shaped structure and TL_4 are optimized by Advanced Design System, and the optimized parameters are as follows: $L_1 = 3.2$ mm, $L_2 = 3.6$ mm, $L_3 = 0.6$ mm, $L_4 = 7.2$ mm, $W_1 = 2.7$ mm, $W_2 = 1.0$ mm, $W_3 = 2.2$ mm, $W_4 = 1$ mm. Fig. 8 depicts the layout of the rectifier circuit.

Figure 9 exhibits the simulated DC voltage and conversion efficiency of the rectifier circuit. The load resistance of the rec-

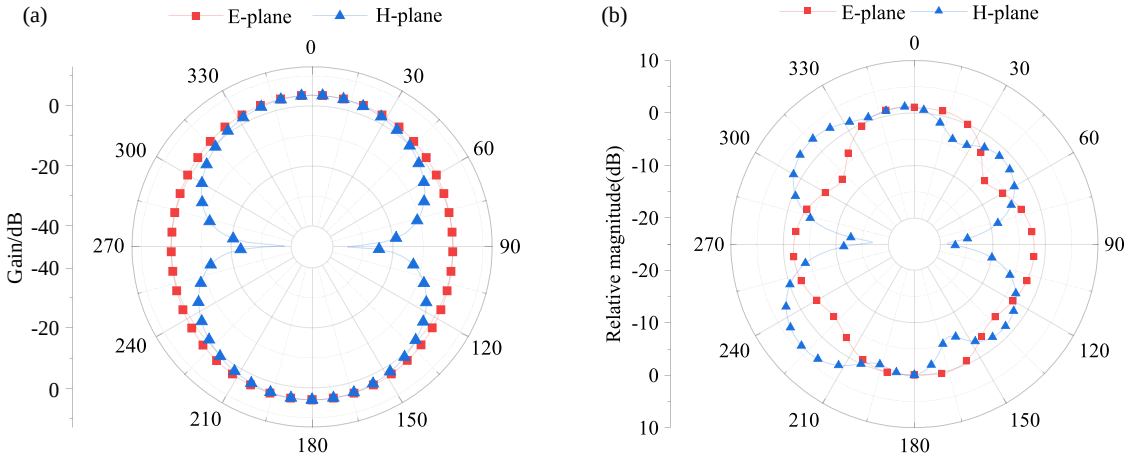

FIGURE 6. Radiation pattern of the antenna 3 (a) 2.45 GHz, (b) 5.8 GHz.

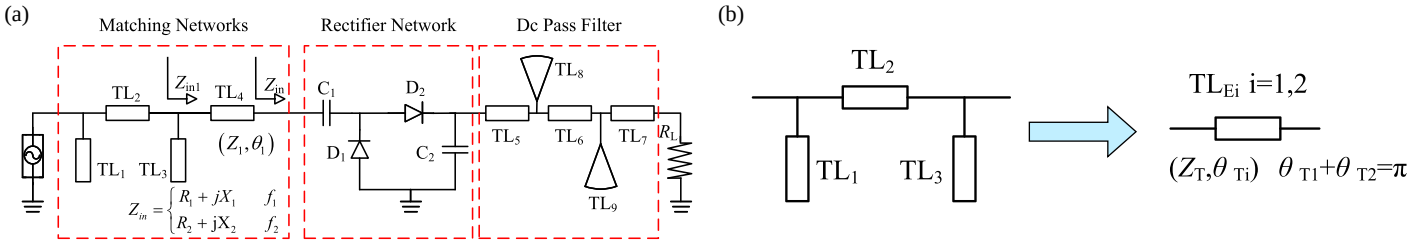

FIGURE 7. Schematic diagram (a) rectifier circuit, (b) Π-shaped network.

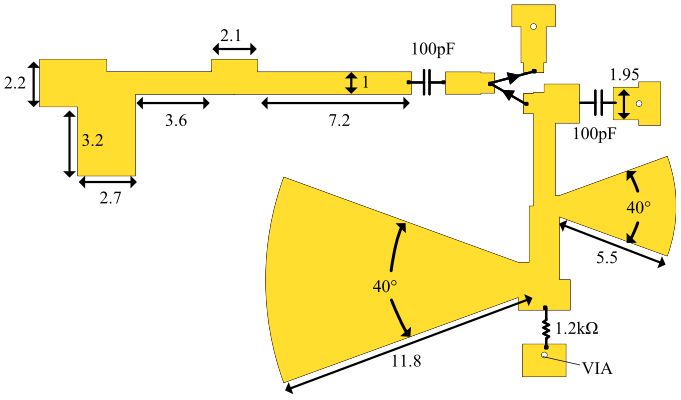

FIGURE 8. Layout of rectifier circuit (unit: mm).

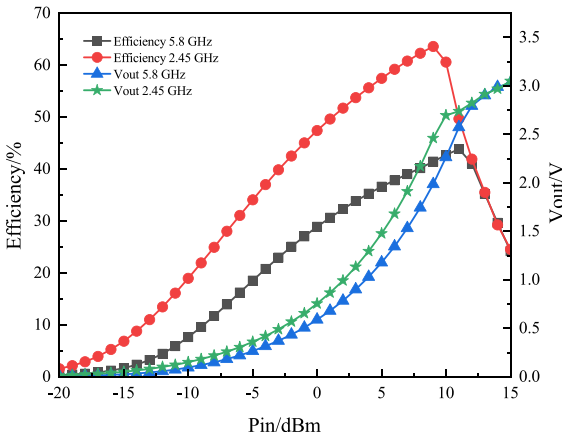

FIGURE 9. Simulated conversion efficiencies and output voltages at different input powers.

tifier circuit is 1.2 kΩ. At 2.45 GHz, the maximum conversion efficiency is 63.6%, and the DC voltage is 2.46 V at an input power of 9 dBm. At 5.8 GHz, the maximum conversion efficiency is 43.8%, and the DC voltage is 2.57 V at an input power of 11 dBm.

3.2. Co-Simulation of the Rectenna

The rectifier circuit is integrated in antenna 3 to form a rectenna, as shown in Fig. 10. To research the change of performance of the antenna after it is integrated in a rectifier circuit, the current distributions of rectenna and antenna are simulated by using EM Circuit Excitation function in Advanced Design System. The current distribution is depicted in Figs. 11. Comparing Fig. 11(a) with Fig. 11(b) and Fig. 11(c) with Fig. 11(d), it can be seen that the current distribution of the antenna barely changes, indicating that the performance of the antenna is hardly changed after connecting the rectifier circuit.

4. TEST AND ANALYSIS

4.1. Test and Analysis of the Antenna

As shown in Fig. 12, antenna 3 was fabricated, and the SMA connector was soldered to antenna 3. Fig. 13 shows S_{11} of the antenna: the simulated impedance bandwidths are 2.06 $\sim$ 2.66 GHz and 5.57 $\sim$ 6.03 GHz, and the S_{11} at 2.45 GHz and 5.8 GHz are -36.3 dB and -45.3 dB, respectively. The mea-

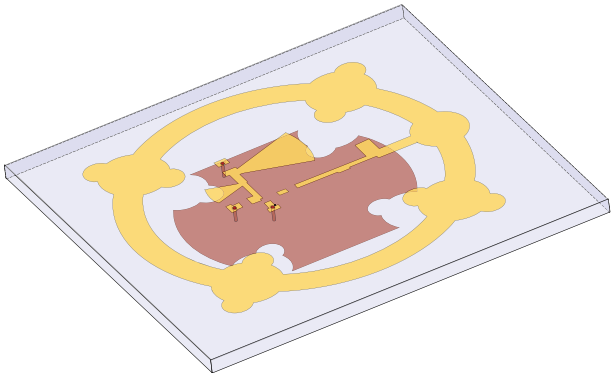

FIGURE 10. Rectenna structure diagram.

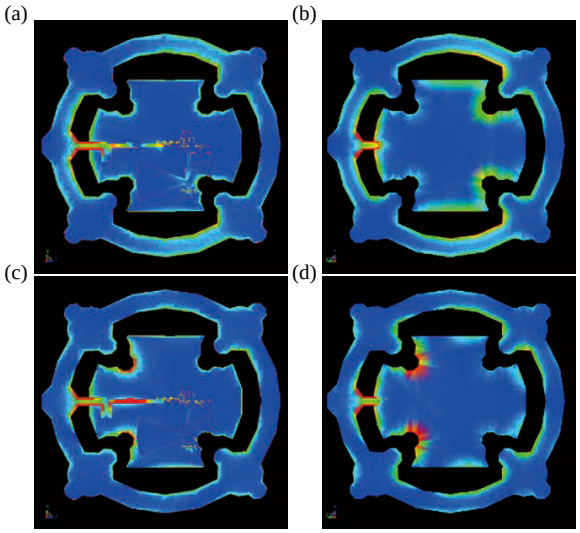

FIGURE 11. Visual current diagram. (a) 2.45 GHz rectenna, (b) 2.45 GHz antenna, (c) 5.8 GHz rectenna, (d) 5.8 GHz antenna.

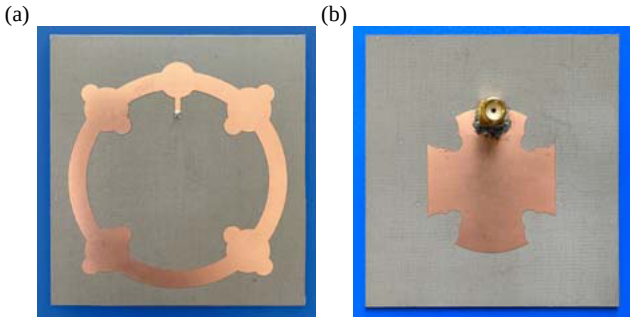

FIGURE 12. Photographs of antenna. (a) Front. (b) Back.

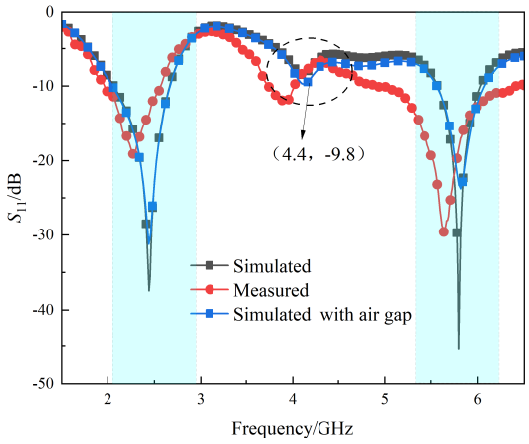

FIGURE 13. Simulated and measured S_{11} of antenna.

sured impedance bandwidths are $2 \sim 2.56$ GHz, $3.75 \sim 4$ GHz, and $5.15 \sim 6.28$ GHz, and S_{11} are -13.5 dB and -18.7 dB at 2.45 GHz and 5.8 GHz, respectively. The simulated and measured radiation patterns of the antenna 3 are shown in Fig. 14. The radiation pattern is omnidirectional at 2.45 GHz and quasi-omnidirectional at 5.8 GHz. The measured and simulated data are similar. Nonetheless, the resonant frequencies are shifted to lower frequencies with a new frequency emerging between the two frequencies. The main reason for the difference between the simulated and measured results is that there is an air gap between the probe and the substrate. The radius of the probe used in the simulation is 0.5 mm, while the radius of the probe used in the test is 0.375 mm, so there is an air gap between the probe and the substrate. To verify my assumption, the model with the air gap is simulated, and the result is shown in Fig. 13. The S_{11} of the antenna drops to -9.8 dBm around 4 GHz. The secondary reasons are the influence of antenna processing accuracy, test environment, and welding accuracy. The results of the test and simulation are similar, and deviations are within acceptable limits.

4.2. Test of Rectifier Circuit

A photograph of the rectifier circuit is shown in Fig. 15, and the dimension of the rectifier circuit is 34.7 mm $\times$ 26 mm $\times$ 1.016 mm. Signals of different powers and frequencies generated by the signal generator are fed into the rectifier circuit through the SMA connector. The DC voltage of the load is measured with a voltmeter. Fig. 16 displays the rectifier circuit's DC voltage and conversion efficiencies at various input powers. With a load of 1.2 kΩ, a peak conversion efficiency of 55.7% and a DC output voltage of 2.9 V are measured at 2.45 GHz when the input power is 11 dBm, and a peak conversion efficiency of 37.1% and a DC output voltage of 2.98 V are measured at 5.8 GHz when the input power is 13 dBm. The tested conversion efficiency at both frequencies has dropped compared to the simulated results, and the following factors are to blame for the inaccuracies: (1) The simulated diode model differs from the actual model; (2) Both chip components and diodes exhibit parasitic effects; (3) Both the tested procedure and machining precision contain inaccuracies.

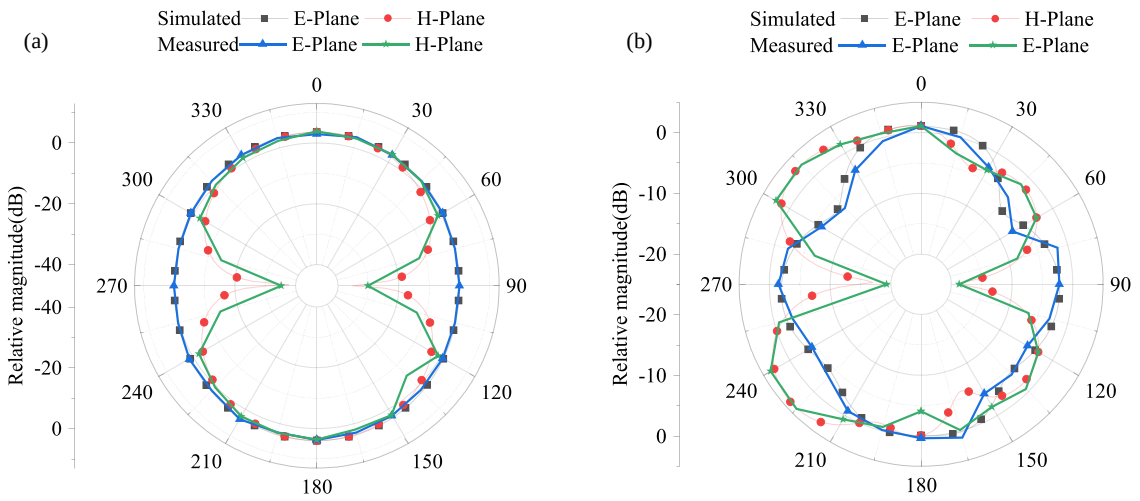

FIGURE 14. Simulated and measured radiation pattern. (a) 2.45 GHz, (b) 5.8 GHz.

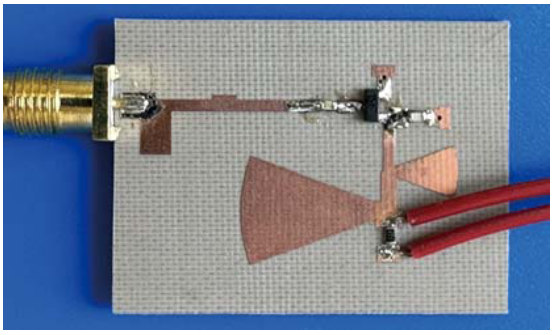

FIGURE 15. Photograph of rectifier circuit.

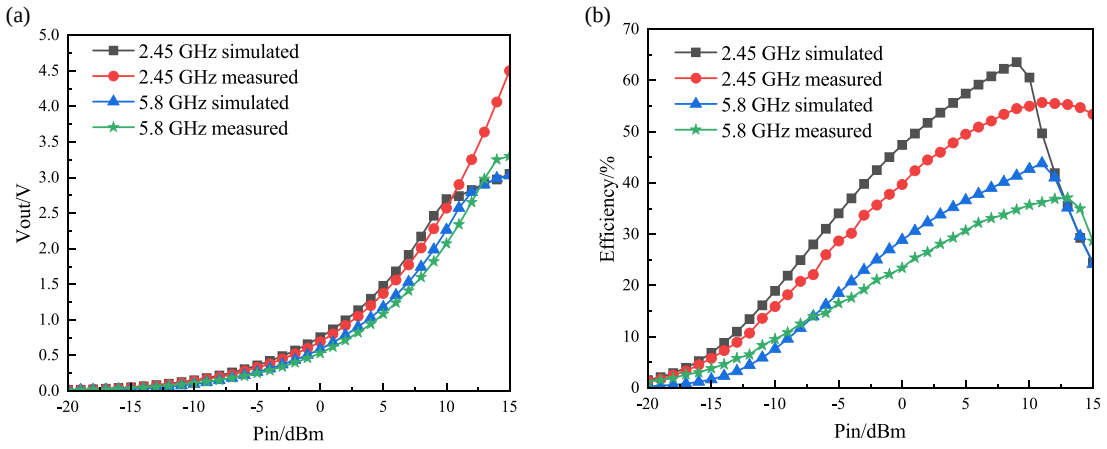

FIGURE 16. Rectifier circuit curves at different input powers. (a) Output voltage curves. (b) Conversion efficiency curves.

4.3. Test of Rectenna

Figure 17 illustrates photographs of the rectenna, which has a dimension of 67.5 mm × 71.5 mm × 1.016 mm. The tested system shown in Fig. 18 is designed to evaluate the RF energy harvesting performance of the rectenna. To reduce the impact of the tested environment on the results, electronic devices such as computers and mobile phones are removed from the tested area. The conversion efficiency of the rectenna can be calculated by Equation (5)

$$\eta = \frac{P_{\text{dc}}}{P_r} \times 100\% = \frac{V_{\text{out}}^2}{R_L P_r} \times 100\% \tag{5}$$

where P_r is the output RF power of the antenna as measured by a spectrum analyzer, P_{dc} the DC power output from the rectifier circuit, V_{out} the voltage of the load measured with a voltmeter, and R_L the load resistance. The RF signal output from

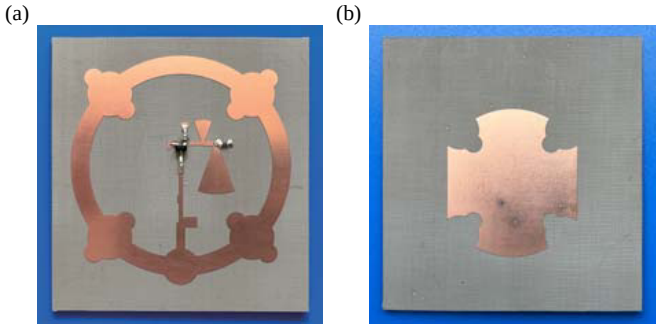

FIGURE 17. Photographs of rectenna. (a) Front. (b) Back.

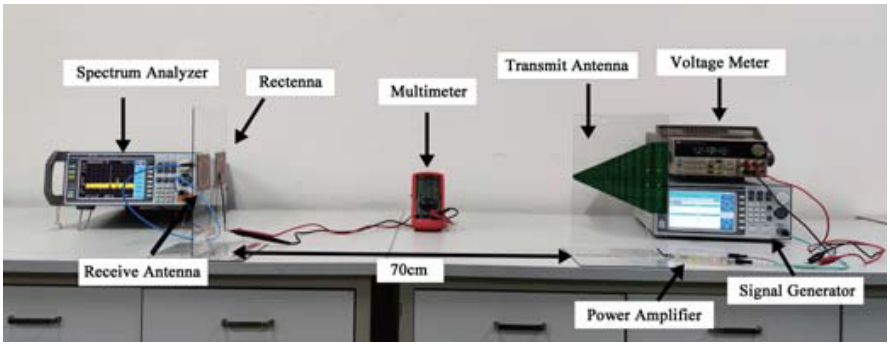

FIGURE 18. Photographs of rectenna test system.

TABLE 2. Comparison of this paper with other research results.

Ref.	f_1 (GHz)	f_1 Eff	f_2 (GHz)	f_2 Eff	Dimension (mm^3)	load (Ω)
[12]	2.4	36%	5.8	8%	$75 \times 75 \times 0.8$	12 kΩ
[13]	2.4	56.3%	5.48	37.8%	$85.6 \times 64 \times 9.2$	1 kΩ
[14]	3.5	44%	5.8	29%	$> 65 \times 95 \times 5$	0.5 kΩ
[15]	2.45	48%	5.8	45%	$200 \times 150 \times 2.8$	5.6 kΩ
[16]	2.4	79.3%	5.8	60%	$133 \times 75 \times 1.524$	1.8 kΩ
[17]	2.4	63%	5.8	54.8%	$80 \times 48 \times 1.6$	0.6 kΩ
[18]	2.45	47.25%	5.8	42%	$103 \times 40 \times 0.787$	3.9 kΩ
This	2.45	65.1%	5.8	38.4%	$67.5 \times 71.5 \times 1.016$	1.2 kΩ

the signal generator is amplified by the power amplifier and radiated into the free space by the log periodic antenna. The spectrum analyzer is connected to antenna 3, located in the far field area to measure the RF power gathered by antenna 3. The log-periodic antenna and antenna 3 keep in good polarization alignment. Concurrently, the rectenna is placed at the same location as antenna 3, and a voltmeter is used to measure the voltage across the load. The far field is the area at a distance greater than $\frac{2D_{\max}^2}{\lambda}$ from the transmitting antenna, where $D_{\max}$ is the maximum dimension of the transmitting and receiving antennas, and λ is the operating wavelength in free space. Therefore, the distance between the transmitting antenna and receiving antenna is set to 70 cm.

Figure 19 depicts the output voltages and conversion efficiencies of the rectenna at various input powers. When input power is 10.5 dBm, the peak conversion efficiency and volt-

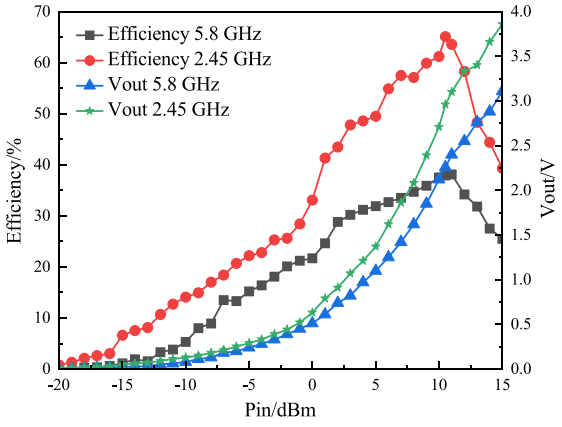

FIGURE 19. Conversion efficiency and output voltage of rectenna at various input powers.

age at 2.45 GHz are 65.1% and 2.96 V, respectively; when input power is 11 dBm, the same values at 5.8 GHz are 38.4% and 2.41 V, respectively.

A comparison of the relevant published results with the results of this paper is presented in Table 2. The size of the rectenna proposed in this paper is smaller than most of the research results (67.5 mm×71.5 mm×1.016 mm); the conversion efficiencies at 2.45 GHz and 5.8 GHz are 65.1% and 38.4%, respectively, which are higher than most of the research results. The proposed rectenna has small size, low profile, and high conversion efficiencies due to the consideration of antenna and rectifier layout.

5. CONCLUSION

This paper proposes a dual-band omnidirectional rectenna with a rectifier circuit integrated in the center of a loop-shaped antenna. The designed rectenna achieves 65.1% and 38.4% conversion efficiencies at 2.45 GHz and 5.8 GHz, respectively, with a rectenna size of 67.5 mm × 71.5 mm × 1.016 mm. The overall size of the rectenna can be reduced by placing the rectifier circuit in the center of the loop-shaped antenna.

ACKNOWLEDGEMENT

This work was supported by the Liaoning Provincial Education Department Scientific Research Funding Program (LJKZ0368) and the National Natural Science Foundation of China (61971210).

REFERENCES

[1] Ertam, F., I. F. Kilincer, O. Yaman, and A. Sengur, "A new IoT application for dynamic WiFi based wireless sensor network," in *2020 International Conference on Electrical Engineering (ICEE)*, 1–4, IEEE, 2020.

[2] Shaikh, F. K. and S. Zeadally, "Energy harvesting in wireless sensor networks: A comprehensive review," *Renewable and Sustainable Energy Reviews*, Vol. 55, 1041–1054, Mar. 2016.

[3] Kamalinejad, P., C. Mahapatra, Z. Sheng, S. Mirabbasi, V. C. M. Leung, and Y. L. Guan, "Wireless energy harvesting for the Internet of Things," *IEEE Communications Magazine*, Vol. 53, No. 6, 102–108, Jun. 2015.

[4] Chandravanshi, S., S. S. Sarma, and M. J. Akhtar, "Design of triple band differential rectenna for RF energy harvesting," *IEEE Transactions on Antennas and Propagation*, Vol. 66, No. 6, 2716–2726, Jun. 2018.

[5] Song, C., Y. Huang, P. Carter, J. Zhou, S. Yuan, Q. Xu, and M. Kod, "A novel six-band dual CP rectenna using improved impedance matching technique for ambient RF energy harvesting," *IEEE Transactions on Antennas and Propagation*, Vol. 64, No. 7, 3160–3171, 2016.

[6] Wang, Q., H. Chu, Y. Dang, J. Qiu, and J. Qi, "A compact 5.8 GHz rectenna with high conversion efficiency enabled by the harmonic suppression for wireless power transfer," in *2022 International Conference on Microwave and Millimeter Wave Technology (ICMMT)*, 1–3, IEEE, 2022.

[7] Dan, Z., Z. He, H. Lin, and C. Liu, "A patch rectenna with an integrated impedance matching network and a harmonic recycling filter," *IEEE Antennas and Wireless Propagation Letters*, Vol. 21, No. 10, 2085–2089, 2022.

[8] Sun, H., "An enhanced rectenna using differentially-fed rectifier for wireless power transmission," *IEEE Antennas and Wireless Propagation Letters*, Vol. 15, 32–35, 2015.

[9] Wang, C., J. Zhang, S. Bai, D. Chang, and L. Duan, "A multiband compact flexible energy collector for wearable or portable IoT devices," *IEEE Antennas and Wireless Propagation Letters*, Vol. 22, No. 5, 1164–1168, 2023.

[10] Wang, Y., J. Zhang, Y. Su, X. Jiang, C. Zhang, L. Wang, and Q. Cheng, "Efficiency enhanced seven-band omnidirectional rectenna for RF energy harvesting," *IEEE Transactions on Antennas and Propagation*, Vol. 70, No. 9, 8473–8484, 2022.

[11] Lu, P., C. Song, and K. M. Huang, "Ultra-wideband rectenna using complementary resonant structure for microwave power transmission and energy harvesting," *IEEE Transactions on Microwave Theory and Techniques*, Vol. 69, No. 7, 3452–3462, 2021.

[12] Mattsson, M., C. I. Kolitsidas, and B. L. G. Jonsson, "Dual-band dual-polarized full-wave rectenna based on differential field sampling," *IEEE Antennas and Wireless Propagation Letters*, Vol. 17, No. 6, 956–959, 2018.

[13] Lin, D.-B., C.-K. Yu, C.-K. Lin, and Y.-H. Lee, "Dual band rectenna with one rectifier," in *2017 International Symposium on Electronics and Smart Devices (ISESD)*, 268–272, IEEE, 2017.

[14] Derbal, M. C. and M. Nedil, "A high gain dual band rectenna for RF energy harvesting applications," *Progress In Electromagnetics Research Letters*, Vol. 90, 29–36, 2020.

[15] Saito, K., E. Nishiyama, and I. Toyoda, "A 2.45- and 5.8-GHz dual-band stacked differential rectenna with high conversion efficiency in low power density environment," *IEEE Open Journal of Antennas and Propagation*, Vol. 3, 627–636, 2022.

[16] Deng, X., P. Yang, S. Chen, and W. Ren, "Design of a 2.4 & 5.8 GHz efficient circularly polarized rectenna for wireless power transfer applications," *Electronics*, Vol. 12, No. 12, 2645, 2023.

[17] Bhatt, K., S. Kumar, P. Kumar, and C. C. Tripathi, "Highly efficient 2.4 and 5.8 GHz dual-band rectenna for energy harvesting applications," *IEEE Antennas and Wireless Propagation Letters*, Vol. 18, No. 12, 2637–2641, 2019.

[18] Le, M. T., D. A. Pham, H. T. Vu, V. D. Ngo, and Q. C. Nguyen, "A novel dual-band ambient RF energy harvesting system for autonomous wireless sensor node application," *The Applied Computational Electromagnetics Society Journal (ACES)*, 1367–1375, 2021.